Vol 18 No 10, October 2009
1674-1056/2009/18(10)/4193–15

Chinese Physics B

© 2009 Chin. Phys. Soc.
and IOP Publishing Ltd

Spin-3/2 Ising model AFM/AFM two-layer lattice with crystal field*

Erhan Albayrak† and Ali Yigit

Department of Physics, Erciyes University, 38039, *Kayseri, Turkey*

(Received 8 January 2009; revised manuscript received 11 April 2009)

The spin-3/2 Ising model is investigated for the case of antiferromagnetic (AFM/AFM) interactions on the two-layer Bethe lattice by using the exact recursion relations in the pairwise approach for given coordination numbers $q = 3$, 4 and 6 when the layers are under the influences of equal external magnetic and equal crystal fields. The ground state (GS) phase diagrams are obtained on the different planes in detail and then the temperature-dependent phase diagrams of the system are calculated accordingly. It is observed that the system presents both second- and first-order phase transitions for all q, therefore, tricritical points. It is also found that the system exhibits double-critical end points and isolated points. The model also presents two Néel temperatures, $T_{\rm N}$, and the existence of which leads to the reentrant behaviour.

Keywords: Bethe lattice, spin, ground state, AFM/AFM, layer, phase
PACC: 0550, 0570F, 0570J

1. Introduction

The ultrathin films, multilayers and superlattices consist of multiple layers of different magnetic substances, therefore, there is a high potential for technological advances in information storage and retrieval and in synthesis of new magnets for a variety of applications. These materials exhibit some interesting novel magnetic properties which include the surface magnetic anisotropy, enhanced surface magnetic moment, surface magnetoelastic coupling, giant magnetoresistance, etc. It is well known that the AFM materials also play a great role in these phenomena. The AFM systems differ from the FM ones in many respects, i.e., it tends to have a more delicate balance between exchange and Zeeman energies as a result of cancelation of the magnetizations of the two sublattices. In addition to this, crystal fields also play an important role in these materials. If the crystal field is strong, the energy difference between the split levels is large. In that case, it is energetically more favourable to put as many electrons into the lower energy level before one starts to fill the higher energy level. Filling all the orbitals in the lower level means one has to pair them up (within each orbital) with opposite spins. The effect of pairing electrons with opposite spin makes no addition to the total spin. This results in a low-spin state.

The theoretical approaches in an attempt to simulate these materials usually involve the lower spin systems such as spin-1/2 and spin-1. But it is well known from the single layered lattice studies that the higher spins, such as spin-3/2, are also very interesting. The spin-3/2 Ising model with only bilinear and biquadratic exchange interactions was introduced earlier[1] to explain phase transitions in $DyVO_4$ and its phase diagram was obtained by the use of the mean-field approximation (MFA). Another one was later introduced to study tricritical properties in ternary fluid mixtures (ethanol-water-carbon-dioxide) which was also solved in the MFA.[2] Since then the spin-3/2 models with different structures have been studied by a great number of exact or approximate techniques, because its critical behaviours are much richer than the ones with lower spin systems. Therefore, the models involving spin-3/2 are good candidates for the technological improvements mentioned above.

Recently, the layered Ising models have been used to simulate the ultrathin films, superlattices, multilayers, etc. The usual way to start such a study is to use the lowest spin system, i.e. spin-1/2, which was studied, for example, by the Monte Carlo (MC) simulation for an Ising model consisting of two ferromagnetic layers with different interaction constants coupled weakly

*Project supported by the Scientific and Technological Research Council of Turkey (TUBITAK) (Grant No 107T358).
†Corresponding author. E-mail: albayrak@erciyes.edu.tr

together,[3] by the corner transfer matrix renormalization group method to calculate the critical points and critical exponents for the two-layer Ising model,[4] by means of a mean-field theory (MFT), a generalized MFT, a scaling approach and high-temperature series expansions[5] and by using the transfer-matrix version of an MFA for the layered Ising model on the simple cubic lattice ($q = 6$).[6] The next spin system is spin-1 for which the crystal field plays a great role in the critical behavioirs of the model, while it has no effect on spin-1/2 systems. Some of studies including the study on the spin-1 system may be listed as follows: The phase diagrams of an FM or a ferrimagnetic bilayer system consisting of two magnetic monolayers with different interaction constants coupled together in a transverse crystal field were studied by the use of the effective field theory (EFT) with correlations,[2−7] the complete global phase diagram was studied by the cluster variational theory within the pair approximation,[8] the order-disorder layering transitions of Blume-Capel model were studied using the MC simulations in the presence of a variable crystal field[9] and so on. Thus, even if the multilayer structures containing lower spins has attracted a great deal of attention, the multilayered spin-3/2 systems have not received enough attention so far. As a result, we could only report a few studies of spin-3/2 system: an Ising model which is equivalent to a two-layer Ising model was introduced and the nature of phases was clarified.[10] Using the linked-cluster series expansions, high-temperature series for the free energy, and the staggered susceptibility of the spin-1 and spin-3/2 Heisenberg antiferromagnetic model on the n-layers cubic lattice films were derived for n=2–7 layers.[11] By using a β-function, the critical phenomenon of a general two-layer Ising model on a square lattice was investigated.[12] The phase diagram of the bilayer Ising model on the Bethe lattice was analysed by using the exact recursion relations in a pairwise approach without and with the crystal field interactions.[13] The periodical arrangements of one layer with spin-1/2 and the other layer with spin-3/2 are examined by the use of the EFT.[14] The transverse crystal field effect of the mixed spin Ising bilayer system was studied by using the EFT with a probability distribution technique.[15] Note also that the multilayer structures, especially the bilayer ones, have been attracting a great deal of interest in FM/FM, AFM/AFM or FM/AFM type intralayer and either FM or AFM type interlayer interactions. In these studies, it is found that the critical behaviours of the systems change and become richer with the increase of spin values, with the change of the bilinear interactions from FM to AFM case, with the inclusion of crystal fields, etc. Thus we expect to find much richer phase diagrams for spin-3/2 AFM/AFM bilayer with the crystal field. This will be clear when we compare our findings for spin-1 and spin-3/2 models at the end of this work.

The exact solutions for the realistic systems on regular lattices are generally unavailable, thus one has to rely on the approximation methods to obtain a qualitative picture for the considered system. Thus, a two-layer Bethe lattice for an Ising model was studied by using an iteration technique.[16] The role of the interlayer coupling between CuO_2 planes in bilayer-group high-T_c superconductors was studied within a simple randomly decorated bilayer Ising model and a Bethe-lattice approach.[17] The behaviour of the Ising thin films through the use of layered Bethe lattices and Husimi trees was studied.[18] The exact phase diagrams of spin-1/2,[19] and spin-1 Ising models on a two-layer Bethe lattice with[20] and without[21] crystal fields for the case of AFM/AFM interactions were studied by using a pairwise approach. Meanwhile, a Bethe lattice is an infinite Cayleytree or a regular tree, i.e. a connected graph without circuits, and historically its name originated from the fact that its partition function was exactly that of an Ising model in the Bethe approximation.[22] In this study the original one-layer lattice is replaced with the two-layer Bethe lattice with the same coordination number q. It should be mentioned that the one-layer Bethe lattice provides exact solutions, of which the results are qualitatively better approximate for the regular lattices than those of solutions obtained by the conventional mean-field theories.[23] We should also point out that the cluster variation method in the pair approximation studies on regular lattices yield results that are exact for the same model on the Bethe lattice.[24] Of course, the Bethe lattice considerations also have some limitations, that is, transition temperature obtained from the model is higher than that for a regular lattice and the predicted critical exponents are not reliable, see Ref.[16] where some more discussions about the Bethe lattices are also given.

In the present work, we analyse a two-layer spin-3/2 Ising model consisting of two Bethe lattices each with a branching ratio of q Ising spins, where one of the layers is laid over the top of the other layer and the two layers are tied together via an interaction be-

tween the vertically aligned spins. The effects of the external magnetic field, crystal field and the intra- and inter-layer interactions are examined for some different values of the coordination numbers, i.e., $q = 3$, 4 and 6. The solution to the problem is obtained by the use of the recursion relations in a pairwise approach iteratively. Thus, in order to obtain the phase diagrams of the model, the ground state (GS) phase diagrams and also the thermal variations of the order-parameters, response functions and free energies are studied in a great detail.

The rest of this study is set up as follows. Section 2 is devoted to the introduction of the two-layer Bethe lattice and its Hamiltonian, and to the formulation of the model. The GS configurations and its phase diagrams are given in Section 3. The last section is given to the illustrations of the phase diagrams and to the summary and discussion.

2. Two-layer Bethe lattice and exact formulations

The spin-3/2 two-layer model is simulated on a Bethe lattice, and a pairwise approach is employed for its investigation. In this approach, an adjacent (nearest-neighbour) NN pair is picked from the deep inside the two-layer lattice, called the central pair, which forms the first-generation spins. This central pair of spins is connected to q NN spin pairs which form the second-generation spins. Each pair of spins in the second-generation is joined to $(q-1)$ NN's. Therefore, in total, the second-generation has $q(q-1)$ NN's which form the third-generation and so on, it goes on to infinity. As a result, each spin has $(q+1)$ NN spins, q from its own layer and one from the adjacent layer.

The Ising Hamiltonian of such a two-layer Bethe lattice under the influence of the crystal field and an external magnetic fields may be given as

$$\begin{aligned}\mathcal{H} = &-J_1 \sum_{\langle ij \rangle} S_i S_j - J_2 \sum_{\langle i'j' \rangle} \sigma_{i'} \sigma_{j'} \\ &- J_3 \sum_{\langle ii' \rangle} S_i \sigma_{i'} - H_1 \sum_i S_i \\ &- H_2 \sum_{i'} \sigma_{i'} - D\Big(\sum_i {S_i}^2 + \sum_{i'} \sigma_{i'}^2 \Big),\end{aligned} \tag{1}$$

where S_i and $\sigma_{i'}$ are spin-3/2 with the values $\pm 3/2$ and $\pm 1/2$ and refer to the spins in the upper, G_1, and lower, G_2, layers, respectively. $J_1 < 0$ and $J_2 < 0$ (for the AFM interaction) are the intralayer bilinear interactions of the NN spins of the layers. Thus, the first and second summations are over all NN sites of G_1 and G_2, respectively. J_3 is the interlayer bilinear interaction of adjacent NN spins between the layers, therefore, the third summation runs over all the adjacent neighbouring sites of G_1 and G_2. The layers are assumed to be under the influence of external magnetic fields H_1 and H_2 and crystal field D, therefore, the last four sums run over all the lattice sites in each layer, respectively. It is necessary to assume that the layers are under the influence of different external magnetic fields to calculate the susceptibility of each layer separately [See Eq.(8)]. As usual, the partition function is defined as

$$\mathbb{Z} = \sum_{\text{All Config.}} \mathrm{e}^{-\beta \mathcal{H}} = \sum_{Spc} P(Spc), \tag{2}$$

where $P(Spc)$ is the unnormalized probability distribution, $\beta = 1/kT$ is the inverse temperature and k is the Boltzmann constant, and the summation runs over all the spin configurations (Spc). Starting from the central pair of spins on the Bethe lattice made up with q separate branches connecting each pair of spins, one follows only one of the branches of the tree out of q, therefore, for the full formulation we have to define the partition function for each of these separate branches called $g_n(S, \sigma)$. It should be mentioned that each spin S_i and spin $\sigma_{i'}$ with spin-3/2 can take the values $\pm 3/2$ and $\pm 1/2$, thus we have to define sixteen $g_n(S, \sigma)$ functions for $4^2 = 16$ configurations for each pair of spins. As a result in this pairwise approach, fifteen exact recursion relations are defined as the ratios of these partition functions of the separate branches on the two-layer Bethe lattice as follows:

$$\begin{aligned}
A_n &= \frac{g_n(\frac{3}{2}, \frac{3}{2})}{g_n(-\frac{1}{2}, -\frac{1}{2})}, \quad B_n = \frac{g_n(\frac{3}{2}, -\frac{3}{2})}{g_n(-\frac{1}{2}, -\frac{1}{2})}, \\
C_n &= \frac{g_n(\frac{3}{2}, \frac{1}{2})}{g_n(-\frac{1}{2}, -\frac{1}{2})}, \quad D_n = \frac{g_n(\frac{3}{2}, -\frac{1}{2})}{g_n(-\frac{1}{2}, -\frac{1}{2})}, \\
E_n &= \frac{g_n(-\frac{3}{2}, \frac{3}{2})}{g_n(-\frac{1}{2}, -\frac{1}{2})}, \quad F_n = \frac{g_n(-\frac{3}{2}, -\frac{3}{2})}{g_n(-\frac{1}{2}, -\frac{1}{2})}, \\
G_n &= \frac{g_n(-\frac{3}{2}, \frac{1}{2})}{g_n(-\frac{1}{2}, -\frac{1}{2})}, \quad H_n = \frac{g_n(-\frac{3}{2}, -\frac{1}{2})}{g_n(-\frac{1}{2}, -\frac{1}{2})}, \\
I_n &= \frac{g_n(\frac{1}{2}, \frac{3}{2})}{g_n(-\frac{1}{2}, -\frac{1}{2})}, \quad J_n = \frac{g_n(\frac{1}{2}, -\frac{3}{2})}{g_n(-\frac{1}{2}, -\frac{1}{2})}, \\
K_n &= \frac{g_n(\frac{1}{2}, \frac{1}{2})}{g_n(-\frac{1}{2}, -\frac{1}{2})}, \quad L_n = \frac{g_n(\frac{1}{2}, -\frac{1}{2})}{g_n(-\frac{1}{2}, -\frac{1}{2})}, \\
M_n &= \frac{g_n(-\frac{1}{2}, \frac{3}{2})}{g_n(-\frac{1}{2}, -\frac{1}{2})}, \quad N_n = \frac{g_n(-\frac{1}{2}, -\frac{3}{2})}{g_n(-\frac{1}{2}, -\frac{1}{2})}, \\
R_n &= \frac{g_n(-\frac{1}{2}, \frac{1}{2})}{g_n(-\frac{1}{2}, -\frac{1}{2})}.
\end{aligned} \tag{3}$$

It should be noted that each recursion relation is a function of the recursion relations for the NN shell with $(n-1)$, therefore in order to obtain their numerical values for given system parameters an iteration method is going to be used. Meanwhile, the choice of the recursion relations, i.e. the ratios of these $g_n(S,\sigma)$ functions, are completely arbitrary. In the thermodynamic limit $(n \to \infty)$ these recursion relations determine the states of the system, and they may be referred to as the equations of state.

The magnetizations M_1 and M_2 of the layers G_1 and G_2, respectively, are the order-parameters and defined respectively as

$$M_1 = \langle S \rangle \quad \texttt{and} \quad M_2 = \langle \sigma \rangle, \tag{4}$$

where $\langle \ldots \rangle$ denotes the usual thermal average. The magnetizations M_1 and M_2 are calculated in terms of the recursion relations as

$$\begin{aligned} M_1 = \{3[&e^{\beta(\frac{9}{4}J_3+\frac{3}{2}H_1+\frac{3}{2}H_2+\frac{9}{2}D)}A_n^q + e^{\beta(-\frac{9}{4}J_3+\frac{3}{2}H_1-\frac{3}{2}H_2+\frac{9}{2}D)}B_n^q \\ &+ e^{\beta(\frac{3}{4}J_3+\frac{3}{2}H_1+\frac{1}{2}H_2+\frac{5}{2}D)}C_n^q + e^{\beta(-\frac{3}{4}J_3+\frac{3}{2}H_1-\frac{1}{2}H_2+\frac{5}{2}D)}D_n^q \\ &- e^{\beta(-\frac{9}{4}J_3-\frac{3}{2}H_1+\frac{3}{2}H_2+\frac{9}{2}D)}E_n^q - e^{\beta(\frac{9}{4}J_3-\frac{3}{2}H_1-\frac{3}{2}H_2+\frac{9}{2}D)}F_n^q \\ &- e^{\beta(-\frac{3}{4}J_3-\frac{3}{2}H_1+\frac{1}{2}H_2+\frac{5}{2}D)}G_n^q - e^{\beta(\frac{3}{4}J_3-\frac{3}{2}H_1-\frac{1}{2}H_2+\frac{5}{2}D)}H_n^q] \\ &+ [e^{\beta(\frac{3}{4}J_3+\frac{1}{2}H_1+\frac{3}{2}H_2+\frac{5}{2}D)}I_n^q + e^{\beta(-\frac{3}{4}J_3+\frac{1}{2}H_1-\frac{3}{2}H_2+\frac{5}{2}D)}J_n^q \\ &+ e^{\beta(\frac{1}{4}J_3+\frac{1}{2}H_1+\frac{1}{2}H_2+\frac{1}{2}D)}K_n^q + e^{\beta(-\frac{1}{4}J_3+\frac{1}{2}H_1-\frac{1}{2}H_2+\frac{1}{2}D)}L_n^q \\ &- e^{\beta(-\frac{3}{4}J_3-\frac{1}{2}H_1+\frac{3}{2}H_2+\frac{5}{2}D)}M_n^q - e^{\beta(\frac{3}{4}J_3-\frac{1}{2}H_1-\frac{3}{2}H_2+\frac{5}{2}D)}N_n^q \\ &- e^{\beta(-\frac{1}{4}J_3-\frac{1}{2}H_1+\frac{1}{2}H_2+\frac{1}{2}D)}R_n^q - e^{\beta(\frac{1}{4}J_3-\frac{1}{2}H_1-\frac{1}{2}H_2+\frac{1}{2}D)}]\}/2\mathbb{Z} \end{aligned} \tag{5}$$

and

$$\begin{aligned} M_2 = \{3[&e^{\beta(\frac{9}{4}J_3+\frac{3}{2}H_1+\frac{3}{2}H_2+\frac{9}{2}D)}A_n^q - e^{\beta(-\frac{9}{4}J_3+\frac{3}{2}H_1-\frac{3}{2}H_2+\frac{9}{2}D)}B_n^q \\ &+ e^{\beta(-\frac{9}{4}J_3-\frac{3}{2}H_1+\frac{3}{2}H_2+\frac{9}{2}D)}E_n^q - e^{\beta(\frac{9}{4}J_3-\frac{3}{2}H_1-\frac{3}{2}H_2+\frac{9}{2}D)}F_n^q \\ &+ e^{\beta(\frac{3}{4}J_3+\frac{1}{2}H_1+\frac{3}{2}H_2+\frac{5}{2}D)}I_n^q - e^{\beta(-\frac{3}{4}J_3+\frac{1}{2}H_1-\frac{3}{2}H_2+\frac{5}{2}D)}J_n^q \\ &+ e^{\beta(-\frac{3}{4}J_3-\frac{1}{2}H_1+\frac{3}{2}H_2+\frac{5}{2}D)}M_n^q - e^{\beta(\frac{3}{4}J_3-\frac{1}{2}H_1-\frac{3}{2}H_2+\frac{5}{2}D)}N_n^q] \\ &+ [e^{\beta(\frac{3}{4}J_3+\frac{3}{2}H_1+\frac{1}{2}H_2+\frac{5}{2}D)}C_n^q - e^{\beta(-\frac{3}{4}J_3+\frac{3}{2}H_1-\frac{1}{2}H_2+\frac{5}{2}D)}D_n^q \\ &+ e^{\beta(-\frac{3}{4}J_3-\frac{3}{2}H_1+\frac{1}{2}H_2+\frac{5}{2}D)}G_n^q - e^{\beta(\frac{3}{4}J_3-\frac{3}{2}H_1+\frac{1}{2}H_2+\frac{5}{2}D)}H_n^q \\ &+ e^{\beta(\frac{1}{4}J_3+\frac{1}{2}H_1+\frac{1}{2}H_2+\frac{1}{2}D)}K_n^q - e^{\beta(-\frac{1}{4}J_3+\frac{1}{2}H_1-\frac{1}{2}H_2+\frac{1}{2}D)}L_n^q \\ &+ e^{\beta(-\frac{1}{4}J_3-\frac{1}{2}H_1+\frac{1}{2}H_2+\frac{1}{2}D)}R_n^q - e^{\beta(\frac{1}{4}J_3-\frac{1}{2}H_1-\frac{1}{2}H_2+\frac{1}{2}D)}]\}/2\mathbb{Z}, \end{aligned} \tag{6}$$

where

$$\begin{aligned} \mathbb{Z} = &e^{\beta(\frac{9}{4}J_3+\frac{3}{2}H_1+\frac{3}{2}H_2+\frac{9}{2}D)}A_n^q + e^{\beta(-\frac{9}{4}J_3+\frac{3}{2}H_1-\frac{3}{2}H_2+\frac{9}{2}D)}B_n^q \\ &+ e^{\beta(\frac{3}{4}J_3+\frac{3}{2}H_1+\frac{1}{2}H_2+\frac{5}{2}D)}C_n^q + e^{\beta(-\frac{3}{4}J_3+\frac{3}{2}H_1-\frac{1}{2}H_2+\frac{5}{2}D)}D_n^q \\ &+ e^{\beta(-\frac{9}{4}J_3-\frac{3}{2}H_1+\frac{3}{2}H_2+\frac{9}{2}D)}E_n^q + e^{\beta(\frac{9}{4}J_3-\frac{3}{2}H_1-\frac{3}{2}H_2+\frac{9}{2}D)}F_n^q \\ &+ e^{\beta(-\frac{3}{4}J_3-\frac{3}{2}H_1+\frac{1}{2}H_2+\frac{5}{2}D)}G_n^q + e^{\beta(\frac{3}{4}J_3-\frac{3}{2}H_1-\frac{1}{2}H_2+\frac{5}{2}D)}H_n^q \\ &+ e^{\beta(\frac{3}{4}J_3+\frac{1}{2}H_1+\frac{3}{2}H_2+\frac{5}{2}D)}I_n^q + e^{\beta(-\frac{3}{4}J_3+\frac{1}{2}H_1-\frac{3}{2}H_2+\frac{5}{2}D)}J_n^q \\ &+ e^{\beta(\frac{1}{4}J_3+\frac{1}{2}H_1+\frac{1}{2}H_2+\frac{1}{2}D)}K_n^q + e^{\beta(-\frac{1}{4}J_3+\frac{1}{2}H_1-\frac{1}{2}H_2+\frac{1}{2}D)}L_n^q \\ &+ e^{\beta(-\frac{3}{4}J_3-\frac{1}{2}H_1+\frac{3}{2}H_2+\frac{5}{2}D)}M_n^q + e^{\beta(\frac{3}{4}J_3-\frac{1}{2}H_1-\frac{3}{2}H_2+\frac{5}{2}D)}N_n^q \\ &+ e^{\beta(-\frac{1}{4}J_3-\frac{1}{2}H_1+\frac{1}{2}H_2+\frac{1}{2}D)}R_n^q + e^{\beta(\frac{1}{4}J_3-\frac{1}{2}H_1-\frac{1}{2}H_2+\frac{1}{2}D)}. \end{aligned} \tag{7}$$

The two response functions are the susceptibility and the specific heat. Thus the constant field susceptibilities of the layers G_1 and G_2 are given by the definition as

$$\chi_{1T} = \lim_{H_1 \to H} \frac{\partial M_1}{\partial H_1} \quad \texttt{and} \quad \chi_{2T} = \lim_{H_2 \to H} \frac{\partial M_2}{\partial H_2}, \tag{8}$$

and the total susceptibility of the two-layer is just the sum of the susceptibilities, i.e.

$$\chi_T = \chi_{1T} + \chi_{2T}. \tag{9}$$

In order to obtain the specific heat, the free energy in terms of the recursion relations is needed. Therefore, the free energy of the two-layer lattice is given as

$$-\beta F = \frac{q}{2}\mathrm{Log}\,\mathbb{W} + \frac{2-q}{2}\mathrm{Log}\,\mathbb{Z}, \tag{10}$$

which is used to find the places of the first-order phase transition temperatures, if any exist, the stable solutions, and where

$$\begin{aligned}\mathbb{W} = {} & \mathrm{e}^{\beta(-\frac{3}{4}J_1-\frac{3}{4}J_2+\frac{9}{4}J_3+\frac{3}{2}H_1+\frac{3}{2}H_2+\frac{9}{2}D)}A_n^p \\ & + \mathrm{e}^{\beta(-\frac{3}{4}J_1+\frac{3}{4}J_2-\frac{9}{4}J_3+\frac{3}{2}H_1-\frac{3}{2}H_2+\frac{9}{2}D)}B_n^p \\ & + \mathrm{e}^{\beta(-\frac{3}{4}J_1-\frac{1}{4}J_2+\frac{3}{4}J_3+\frac{3}{2}H_1+\frac{1}{2}H_2+\frac{5}{2}D)}C_n^p \\ & + \mathrm{e}^{\beta(-\frac{3}{4}J_1+\frac{1}{4}J_2-\frac{3}{4}J_3+\frac{3}{2}H_1-\frac{1}{2}H_2+\frac{5}{2}D)}D_n^p \\ & + \mathrm{e}^{\beta(\frac{3}{4}J_1-\frac{3}{4}J_2-\frac{9}{4}J_3-\frac{3}{2}H_1+\frac{3}{2}H_2+\frac{9}{2}D)}E_n^p \\ & + \mathrm{e}^{\beta(\frac{3}{4}J_1+\frac{3}{4}J_2+\frac{9}{4}J_3-\frac{3}{2}H_1-\frac{3}{2}H_2+\frac{9}{2}D)}F_n^p \\ & + \mathrm{e}^{\beta(\frac{3}{4}J_1-\frac{1}{4}J_2-\frac{3}{4}J_3-\frac{3}{2}H_1+\frac{1}{2}H_2+\frac{5}{2}D)}G_n^p \\ & + \mathrm{e}^{\beta(\frac{3}{4}J_1+\frac{1}{4}J_2+\frac{3}{4}J_3-\frac{3}{2}H_1-\frac{1}{2}H_2+\frac{5}{2}D)}H_n^p \\ & + \mathrm{e}^{\beta(-\frac{1}{4}J_1-\frac{3}{4}J_2+\frac{3}{4}J_3+\frac{1}{2}H_1+\frac{3}{2}H_2+\frac{5}{2}D)}I_n^p \\ & + \mathrm{e}^{\beta(-\frac{1}{4}J_1+\frac{3}{4}J_2-\frac{3}{4}J_3+\frac{1}{2}H_1-\frac{3}{2}H_2+\frac{5}{2}D)}J_n^p \\ & + \mathrm{e}^{\beta(-\frac{1}{4}J_1-\frac{1}{4}J_2+\frac{1}{4}J_3+\frac{1}{2}H_1+\frac{1}{2}H_2+\frac{1}{2}D)}K_n^p \\ & + \mathrm{e}^{\beta(-\frac{1}{4}J_1+\frac{1}{4}J_2-\frac{1}{4}J_3+\frac{1}{2}H_1-\frac{1}{2}H_2+\frac{1}{2}D)}L_n^p \\ & + \mathrm{e}^{\beta(\frac{1}{4}J_1-\frac{3}{4}J_2-\frac{3}{4}J_3-\frac{1}{2}H_1+\frac{3}{2}H_2+\frac{5}{2}D)}M_n^p \\ & + \mathrm{e}^{\beta(\frac{1}{4}J_1+\frac{3}{4}J_2+\frac{3}{4}J_3-\frac{1}{2}H_1-\frac{3}{2}H_2+\frac{5}{2}D)}N_n^p \\ & + \mathrm{e}^{\beta(\frac{1}{4}J_1-\frac{1}{4}J_2-\frac{1}{4}J_3-\frac{1}{2}H_1+\frac{1}{2}H_2+\frac{1}{2}D)}R_n^p \\ & + \mathrm{e}^{\beta(\frac{1}{4}J_1+\frac{1}{4}J_2+\frac{1}{4}J_3-\frac{1}{2}H_1-\frac{1}{2}H_2+\frac{1}{2}D)}, \end{aligned} \tag{11}$$

where $p = q - 1$. As a result, the specific heat at constant magnetic field is defined as

$$C_H = T\left(\frac{\partial S}{\partial T}\right)_H = -T\left(\frac{\partial^2 F}{\partial T^2}\right)_H, \tag{12}$$

where H refers to both H_1 and H_2, and S is the entropy and it may be given in a more suitable form as

$$C/k = -\beta'\left[2\beta'\frac{\partial(F/J_i)}{\partial\beta'} + \beta'^2\frac{\partial^2(F/J_i)}{\partial\beta'^2}\right], \tag{13}$$

where $i = 1$ or 2, i.e. J_i refers to intralayer interaction of the upper or lower layer, respectively, and which is not as simple as it is seen, since it includes the first- and second-partial derivatives of the recursion relations with respect to $\beta' = \beta J_i$, therefore, the explicit equation is too long to be given here.

So far we have only obtained the formulations for general interactions, but the layers are assumed to have AFM interactions, therefore, we have to divide layers into sublattices A and B. Hence, the recursion relations for each layer in terms of the sublattices may be written as follows:

$$\begin{aligned} & \{A_n, B_n, \ldots, N_n, R_n\} \\ \rightarrow & \begin{cases} \{A_n^A, B_n^A, \ldots, N_n^A, R_n^A\} & \text{for even } n, \\ \{A_n^B, B_n^B, \ldots, N_n^B, R_n^B\} & \text{for odd } n. \end{cases} \end{aligned} \tag{14}$$

The notable point of this approach is that non-staggered phases are described by the single fixed points $\{A_n, B_n, \ldots, N_n, R_n\} \rightarrow \{A, B, \ldots, N, R\}$, while the staggered phases appear as two-cycle double points as indicated above.

In addition, the sublattice magnetizations for the layers G_1 and G_2, since each spin only interacts with its NN's from its own layer and an NN from the adjacent layer with the same sublattice, i.e. A or B, could be written as

$$\{M_{1,2}\} \rightarrow \begin{cases} \{M_{1A}, M_{2A}\} & \text{for even } n, \\ \{M_{1B}, M_{2B}\} & \text{for odd } n. \end{cases} \tag{15}$$

The free energies of the sublattices are of the form

$$\{F(A_n, \ldots, R_n)\} \rightarrow \begin{cases} \{F(A_n^A, \ldots, R_n^A)\} & \text{for even } n, \\ \{F(A_n^B, \ldots, R_n^B)\} & \text{for odd } n, \end{cases} \tag{16}$$

and then the specific heat is to be defined accordingly, that is

$$\{C(A_n, \ldots, R_n)\} \rightarrow \begin{cases} \{C(A_n^A, \ldots, R_n^A)\} & \text{for even } n, \\ \{C(A_n^B, \ldots, R_n^B)\} & \text{for odd } n. \end{cases} \tag{17}$$

And finally the susceptibility is given as

$$\begin{aligned} & \{\chi(A_n, \ldots, R_n)\} \\ \rightarrow & \begin{cases} \{\chi_1(A_n^A, \ldots, R_n^A) + \chi_2(A_n^A, \ldots, R_n^A)\} & \text{for even } n, \\ \{\chi_1(A_n^B, \ldots, R_n^B) + \chi_2(A_n^B, \ldots, R_n^B)\} & \text{for odd } n. \end{cases} \end{aligned} \tag{18}$$

The next section is devoted to the obtaining of the GS phase diagrams.

3. The ground states phase diagrams

In this Section, the GS phase diagrams are calculated in order to determine zero absolute temperature behaviour of the stable solutions of the model.

Although the GS phase diagrams can only help us at zero temperature, the zero temperature configurations are very important as a starting point in obtaining the temperature-dependent phase diagrams.

The GS phase diagrams are obtained on the $(H/q|J|, J_3/q|J|)$ and $(D/q|J|,\ J_3/q|J|)$ planes for given values of $D/q|J|$ and $H/q|J|$, respectively, on the assumption that $H_1 = H_2 = H$ and $J_1 = J_2 = -J$. They are obtained from expression (1) in units of $|J|$ by rewriting it as:

$$\frac{E}{q|J|} = -\sum_{\langle \text{plaq} \rangle} \left[\frac{J_1}{|J|} S_i S_j + \frac{J_2}{|J|} \sigma_{i'} \sigma_{j'} + \frac{J_3}{q|J|} (S_i \sigma_{i'} + S_j \sigma_{j'}) + \frac{H}{q|J|} (S_i + S_j + \sigma_{i'} + \sigma_{j'}) + \frac{D}{q|J|} (S_i^2 + S_j^2 + \sigma_{i'}^2 + \sigma_{j'}^2) \right], \qquad (19)$$

where the summation is over all the central plaquette which consists of four NN pairs of the two-layer system with one pair $\langle ij \rangle$ from layer G_1, one pair $\langle i'j' \rangle$ from layer G_2, and two pairs $\langle ii' \rangle$ and $\langle jj' \rangle$ connecting layers G_1 and G_2 between the adjacent spins only. The GS phase diagrams are calculated by comparing the values of the energy for different spin configurations and then the GS configurations are the ones with the lowest energy. The coordination number q is hidden in the GS energy equations, thus they are obtained for general q. Only the positive values of $H/q|J|$ is taken, then there is a preferred direction in space. For negative values of $H/q|J|$ the magnetizations only change sign because of the symmetry requirement, $M(-H) = -M(H)$. So, the system exhibits the following ten different types of GS configurations:

I	+3/2 +3/2 +3/2 +3/2
IV	+3/2 +1/2 +3/2 +1/2
VII	+3/2 −1/2 −1/2 +3/2
X	+1/2 +1/2 +1/2 +1/2

II	±3/2 ∓3/2 ∓3/2 ±3/2
V	+3/2 +1/2 +1/2 +3/2
VIII	±1/2 ∓1/2 ±1/2 ∓1/2

III	±3/2 ∓3/2 ±3/2 ∓3/2
VI	+3/2 −1/2 +3/2 −1/2
IX	±1/2 ∓1/2 ∓1/2 ±1/2

Phases I and X are the FM phases and the phases II and IX are the AFM phases for the spin-3/2 and spin-1/2, respectively. While the phases IV and V are the ferrimagnetic phases, phase VII is the antiferrimagnetic phase as seen from the table above. Lastly, phases III and VIII are mixed FM phases for the spin-3/2 and spin-1/2, respectively, the phase VI is the mixed ferrimagnetic phase. Below, we give only the distinct types of the GS phase diagrams of the model.

The first GS phase diagrams are obtained on the $(H/q|J|, J_3/q|J|)$ planes by varying the $D/q|J|$ values and presented in Fig.1. Figure 1(a) is obtained for $D/q|J|$=0.25 and only the three phases, I, II and III are shown. The multiphase lines separate the phases (I, III), (II, III) and (I, II). It may be thought that the phases I and II must be separated by a multiphase line along $J_3/q|J| = 0$ line, but the strong magnetic fields make the spins in phase II align with its NN to form phase I at lower $J_3/q|J|$. Therefore, phase I persists at lower negative $J_3/q|J|$ values also. Note that the phase diagrams for $D/q|J| \geq$0.0 are always the same. Figure 1(b) is obtained for $D/q|J|$=–0.25, in which the multiphase line separating the phases I and II of the previous figure is split into the phases V and VII. This makes sense since there is a smooth transition from phase II to phase I, since antiferrimagnetic phase VII and ferrimagnetic phase V are the neighbours of the phases II and I, respectively. The phases IV and VI are also seen in the form of a triangle separating the phases I and III at lower positive $J_3/q|J|$. So the transitions from phase III (mixed ferro) to VI (mixed ferri) and then from VI to IV (ferri) and finally from IV to I (ferro), are also very reasonable. Note also that

as $D/q|J|$ increases negatively, the areas covered by these configurations increase as shown in the inset obtained for $D/q|J|$=–0.5. The next distinct type of GS phase diagram, figure 1(c), on this plane is obtained for $D/q|J| = -1.0$. Now the phases II and III are split by the phases VIII and IX and have the similar types with III and II, respectively, and which are split by the $J_3/q|J| = 0$ line. Phase X also appears from the middle of the phases VI, IV, V and VII of the previous figure. For further lower values of $D/q|J|$, the GS phase diagrams remains unchanged.

The final GS phase diagrams are obtained on the $(D/q|J|, J_3/q|J|)$ planes by varying the $H/q|J|$ values and presented in Fig.2. The first one, figure 2(a), is obtained for $H/q|J|$=0.2 and in the inset $H/q|J|$=0.5. Phases II and III, and phases VIII and IX are separated with a multiphase line along $J_3/q|J| = 0$ at higher and lower $D/q|J|$ values. In addition, phases III and VIII, and phases II and IX are separated with symmetrical multiphase lines. The same phase dia-

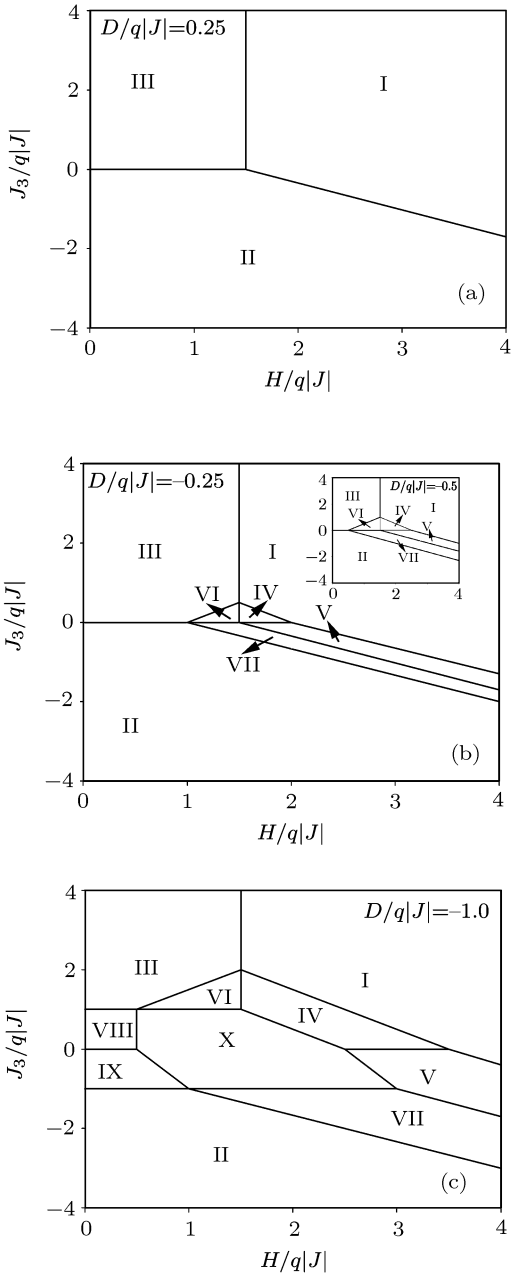


Fig.1. GS phase diagrams of the AFM/AFM spin-3/2 Ising model on the $(H/q|J|, J_3/q|J|)$ planes; (a) $D/q|J| = 0.25$, (b) $D/q|J| = -0.25$ and in the inset $D/q|J| = -0.5$ and (c) $D/q|J| = -1.0$.

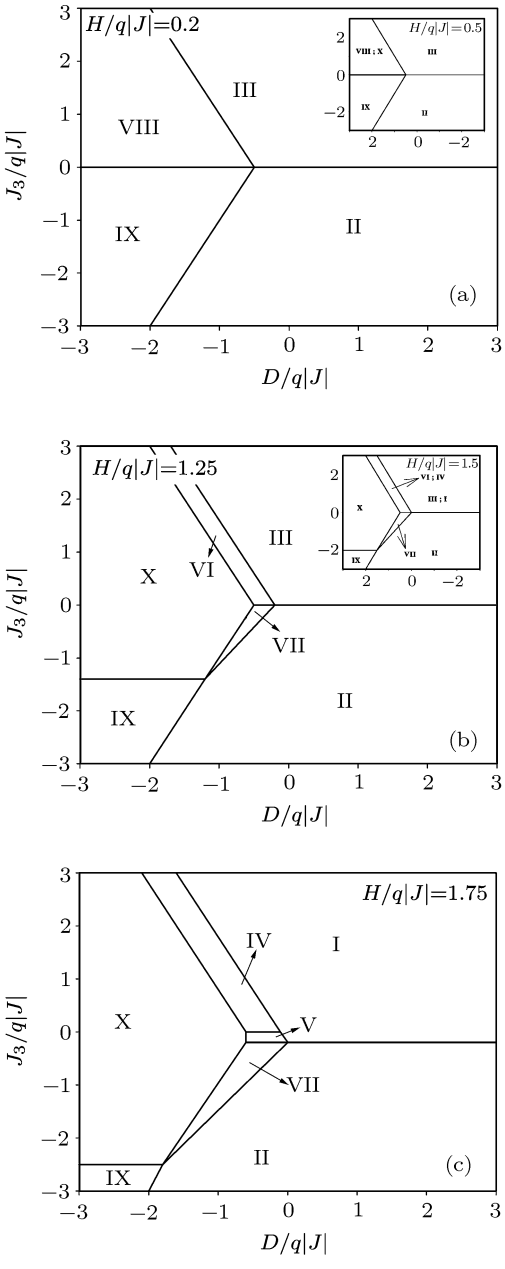


Fig.2. GS phase diagrams of the two-layer Bethe lattice with crystal field for spin-3/2 Ising model on $(D/q|J|, J_3/q|J|)$ planes; (a) $H/q|J| = 0.2$ and in the inset $H/q|J| = 0.5$, (b) $H/q|J| = 1.25$ and in the inset $H/q|J| = 1.5$ and (c) $H/q|J| = 1.75$.

gram continues until $H/q|J|$=0.5 at which phases VIII and X coexist together as seen in the inset, which is interesting. Our next distinct GS phase diagram, figure 2(b), is obtained for $H/q|J|$=1.25 and in the inset for $H/q|J|$=1.5. In the main figure, phases II and III are separated with a multiphase line along $J_3/q|J| = 0$ as in Fig.2(a), but now phases VIII and IX of Fig.2(a) are replaced with phases X and IX which are separated with multiphase lines seen at lower $J_3/q|J|$ for higher $H/q|J|$ (see the inset). In addition to this, while phases III and X are separated with phase VI, phases II and X are separated with phase VII. The inset for $H/q|J|$=1.5 is similar to the main figure but now phases VI and IV, and phases I and III coexist in the same regions of the phase diagrams. In the last phase diagram, figure 2(c) obtained for $H/q|J|$=1.75 is similar to the previous figure, but phases VI and III have disappeared. Furthermore, phases IV and VII are separated with the phase V. The further increase of $H/q|J|$ does not cause any changes in the GS phase diagrams.

These are all the distinct types of the GS phase diagrams of the spin-3/2 Ising model, which are to be used as our guide in obtaining the temperature-dependent phase diagrams. The next section is devoted to the obtaining of the temperature-dependent phase diagrams, which are accomplished by studying the temperature variations of the order-parameters, response functions and free energy, and the nature of the phase transitions are determined from their thermal behaviours.

4. The temperature-dependent phase diagrams

In the light of the previous sections, we are now ready to give some of the distinct phase diagrams of the model. In the phase diagrams the T_N-lines, the lines of the second-order phase transition temperatures, are indicated with gray solid, dash-dotted and solid lines for q = 3, 4 and 6, respectively. Similarly, the arrows indicate the phase separation points according to the GS phase diagrams. The T_t-lines are shown with dash lines. The triangles ($\triangle$) indicate the tricritical points at which the second-order line ends and the first-order line starts. The connection points of two T_t-lines are the double-critical end points ($\bullet$) and the isolated points ($\circ$) where T_t-lines terminate. For simplicity, the obtained phase diagrams are classified according to the obtained planes, i.e. Type A: on the $(J_3/|J|, kT/|J|)$ plane for given $D/q|J|$ and $H/q|J|$; Type B: on the $(H/|J|, kT/|J|)$ plane for given $D/q|J|$ and $J_3/q|J|$ and Type C: on the $(D/|J|, kT/|J|)$ plane for given $H/q|J|$ and $J_3/q|J|$. The possible phase transitions involve phases (II, III), (II, VII, VI, III), (II, VII, V, IV, I), (II, VII, V, I), (III, I), (III, VI, IV, I), (II, IX, VIII, III), (II, IX, X, VI, III), (II, VII, X, VI, III), (II, VII, X, IV, I), (II, VII, X, V, VI, I), (VIII, X, IV, I), (IX, X, V, I), (IX, VIII), (VIII, III), (IX, II), (IX, X), (X, VI, III), (X, VII, II), (X, IV, I), (X, V, I), (II, IX, X, IV, I) and (II, I) and they are labeled as 1,2,... ,23, respectively. For example A1 is understood as the phase diagram on the $(J_3/|J|, kT/|J|)$ plane involving the phases (II, III), etc. In addition, A1(1b), for example, is understood as the phase diagram obtained according to the GS phase diagram Fig.1b, etc.

Our first phase diagram, Fig.(3), is for A1(1b) type and obtained for $H/q|J| = 0.5$ and $D/q|J| = -0.25$. The T_N-lines separate ordered phases, II and III, from the paramagnetic (P) phase. As seen they are constant at higher negative values of $J_3/|J|$, and they are at higher temperatures for higher q. As $J_3/|J|$ increases the T_N's decrease and T_N-lines present concavities for all q about $J_3/|J|$=0.0. As $J_3/|J|$ increases further, they increase and become constant at some temperatures again. Thus the T_N lines have a wing shape each. The arrows indicate phase separation points for all q according to GS Fig.1(b). A1(2b) for $H/q|J| = 1.25$ and $D/q|J| = 1.5$ and A1(2a) for $H/q|J| = 0.2$ and $D/q|J| = 1.0$ are similar to the type A1(1b). It is found that the higher the $D/q|J|$ is, the higher the critical temperatures of the wings will be. The inset is for A14(2a) type and obtained for $H/q|J| = 0.2$ and $D/q|J| = -2.5$, which is similar to the main figure, but the centre of the wings are much sharper and the T_t lines are also seen for all q. They start from just underneath the centre of the concavities and terminate at higher negative values of $J_3/|J|$ for higher q at zero temperature. Note also that A2(1b) for $H/q|J| = 1.35$ and $D/q|J| = -0.25$ and A2(2b) for $H/q|J| = 1.25$ and $D/q|J| = -0.4$ are also similar to A14(2a).

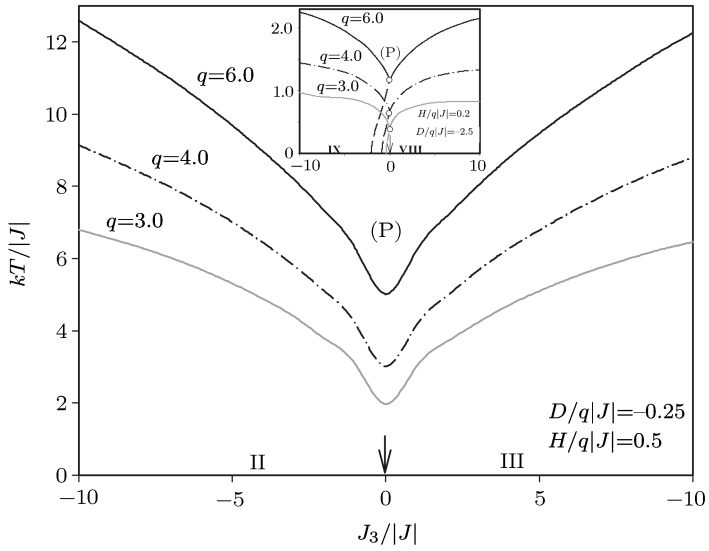
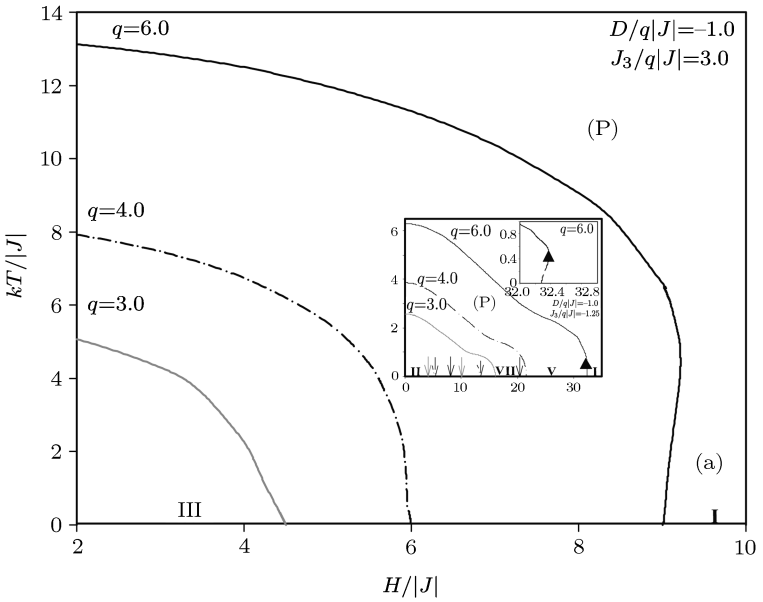


Fig.3. Phase diagrams of type A1(1b) and in the inset type A14(2a) for $D/q|J| = -0.25, -2.5$ and $H/q|J| = 0.5$ and 0.2, respectively.

Figure 4(a) is for B5(1c) type and obtained for $D/q|J| = -1.0$ and $J_3/q|J| = 3.0$. The T_N lines start from higher temperatures for higher q at $H/|J| = 0.0$ and as $H/|J|$ increases their temperatures decrease and they go to zero temperatures at lower $H/|J|$ for lower q. Similar phase diagrams are also found for B5(1b), B6(1c) and B6(1b) when $D/q|J| = -0.25, -1.0, -0.25$ and $J_3/q|J| = 3.0, 1.5, 0.25$, respectively. It is found that the T_N lines start from higher temperatures for higher $J_3/q|J|$ at $H/|J| = 0.0$ but they terminate at lower $H/|J|$ for higher $J_3/q|J|$ at zero temperature. Similarly, the lower the $D/q|J|$ is, the higher the T_N's will be, but their termination $H/|J|$ values do not change. The reentrant behaviour is also observed for only $q = 6$ in all the phase diagrams. The inset with $D/q|J| = -1.0$ and $J_3/q|J| = -1.25$ is for B4(1c) type and similar to Fig.4(a), but the T_t line and a tricritical point are also exhibited when $q = 6$ and the T_N lines are wavy by comparison. The B4(1b) for $D/q|J| = -0.25$ and $J_3/q|J| = -0.5$ is also similar to the inset but now the T_N line for $q = 6$ also presents reentrant behaviour in a range close to the tricritical point. Figure 4(b) (A17(2b) type) for $D/q|J| = -2.5$ and $H/q|J| = 1.25$ resembles the inset of Fig.4(a), i.e. only T_N lines for $q = 3$ and 4, in addition to T_N line with reentrant behaviour, the T_t line and tricritical point are also exhibited when $q = 6$, but now these



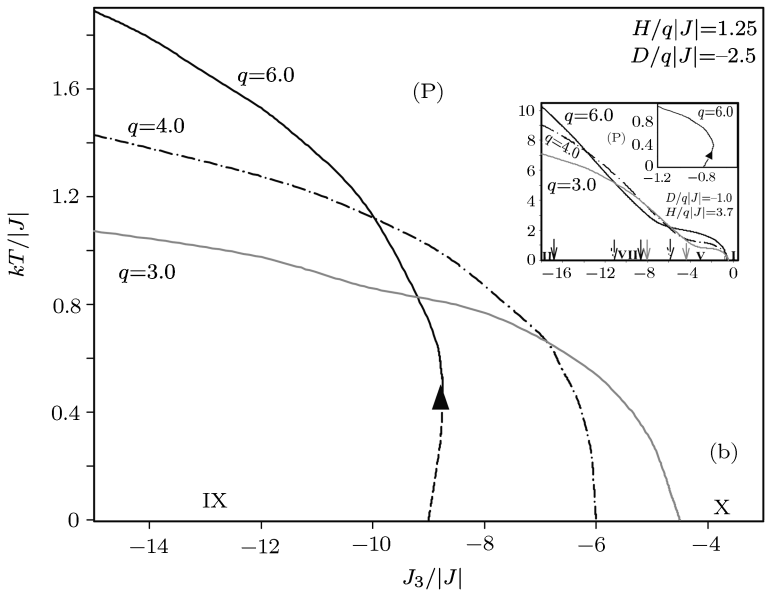


Fig.4. Phase diagrams; (a) Type B5(1c) and in inset type B4(1c) with $D/q|J| = -1.0$ and $J_3/q|J| = 3.0$ and –1.25, respectively. (b) Type A17(2b) and in inset type A4(1c) for $H/q|J| = 1.25$ and 3.7 and $D/q|J| = -2.5$ and -1.0, respectively.

lines go to zero temperature at higher negative $J_3/|J|$ for higher q. The inset is for A4(1c) type and is obtained for $D/q|J| = -1.0$ and $H/q|J| = 3.7$ similar to Fig.4(b), but now again the T_N lines have wavy forms. Note also that the A4(1b), A23(2c) and A17(2c) type phase diagrams for $D/q|J| = -0.25, 1.0, -2.5$ and $H/q|J| = 2.5, 1.75, 1.75$, respectively, are also similar to Fig.4(b). It is seen that for the latter two types, the critical lines go to zero temperature at higher negative $J_3/|J|$ for lower $D/q|J|$ at equal $H/q|J|$'s.

The next phase diagram is for C20(2c) type (see Fig.5), and is obtained for $H/q|J| = 1.75$ and $J_3/q|J| = 2.0$. Since phases I and X are the FM phases, the system does not give any phase transitions when there are external magnetic fields acting on the layers, indeed this is the case. The semi-ellipsoidal shape T_N lines for all q separate the P phase from the phase IV. The semi-ellipsoids move from right towards lower negative $D/|J|$ values and the peaks are seen at lower $kT/|J|$ for lower q. The reentrant behaviour is only seen for $q = 6$ on the two legs of the ellipsoid. The inset ($H/q|J| = 1.75$ and $J_3/q|J| = -0.1$) is for C21(2c) type and similar to the main

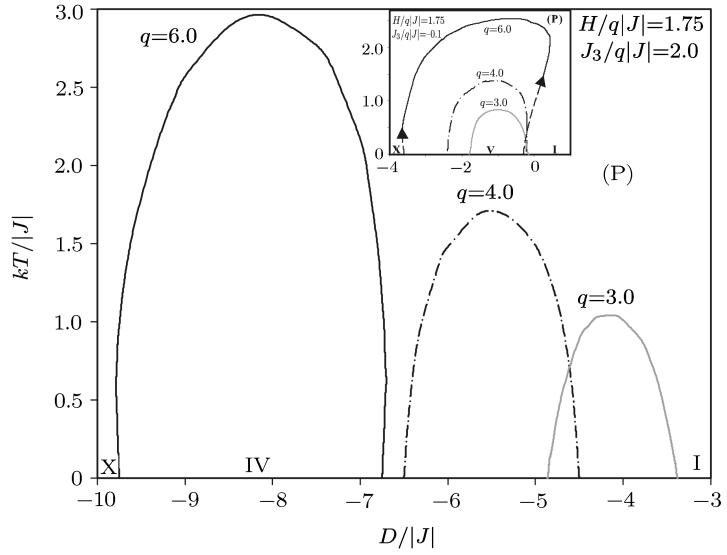


Fig.5. Phase diagrams of type C20(2c) and in the inset for type C21(2c) with $H/q|J| = 1.75$ and $J_3/q|J| = 2.0$ and -0.1, respectively.

figure, but now the ellipsoids are inside one another from the higher q to the lower one. The left legs of these lines also behave similarly, but right legs go to zero temperature at lower $D/|J|$ values for higher q in opposition to the main figure. The T_t lines, shorter on the left and longer on the right, and tricritical points are also found for $q = 6$. The reentrant behaviour on the T_N lines are also observed on both legs for $q = 6$ and on the right leg for $q = 4$, the latter is observed for the first time.

Figure 6 is for C19(2b) type with $H/q|J| = 1.25$ and $J_3/q|J| = -0.5$. The T_N lines at higher temperatures for higher q are at constant temperatures for higher $D/|J|$, but as $D/|J|$ becomes smaller, their temperatures turn lower and the drop becomes more apparent at negative $D/|J|$. The T_N lines terminate at tricritical points, which are seen at higher $kT/|J|$ for higher q, where the T_t lines emerge and end at higher negative $D/|J|$ for higher q. The shapes of the phase diagrams for C19(2c) and C18(2b) types for $H/q|J| = 1.75, 1.25$ and $J_3/q|J| = -1.5, 2.0$, respectively, are similar to Fig.6. For the latter the T_N lines are at higher temperatures for the same $D/|J|$ and the T_t lines terminate at lower $D/|J|$ for higher $J_3/q|J|$.

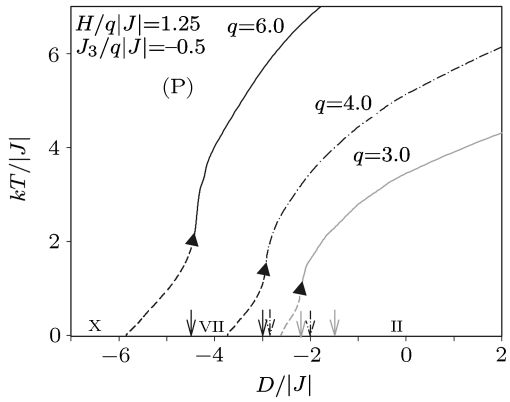


Fig.6. Phase diagram of type C19(2b) for $H/q|J| = 1.25$ and $J_3/q|J| = -0.5$.

The next phase diagram, Fig.7, is obtained for $H/q|J| = 0.2$ and $J_3/q|J| = 1.0$ and it is for C15(2a) type. This phase diagram is similar to the phase diagrams of a single layer spin-3/2 Ising models.[25] The T_N lines start from lower constant temperatures, which are higher for higher q and separate the phase VIII from the P phase, at higher negative $D/|J|$ values; as $D/|J|$ values increase towards right they start rising up, which occurs at lower $D/|J|$ for higher q; if $D/|J|$ increases further they again reach constant temperatures which are at higher $kT/|J|$ for higher q and separate P and III phases from each other. Phases VIII and III are separated with T_t lines starting from zero temperature and ending at isolated points (○), which are at higher $kT/|J|$ for higher q. The inset for $H/q|J| = 0.2$ and $J_3/q|J| = -1.0$ is for C16(2a) type, of which T_N lines are similar to those in Fig.7 but at little higher temperatures. Two T_t lines combined at double-critical end points are observed in the shape looking like a triangle inside which phases II and IX coexist. They are formed at higher negative $D/|J|$ and at higher $kT/|J|$ for higher q. A similar phase diagram with the inset is obtained for $H/q|J| = 1.25$ and $J_3/q|J| = -2.0$, and it is for C16(2b) type and for which the double-critical end points are seen at lower $D/|J|$ by comparison.

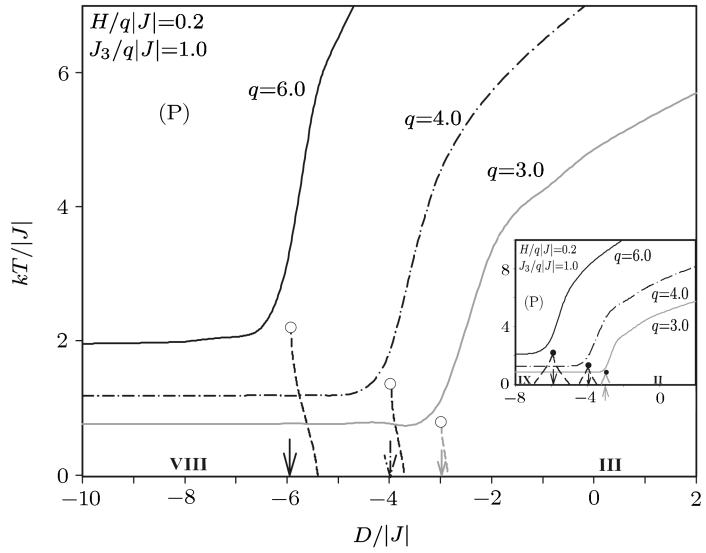


Fig.7. Phase diagrams of type C15(2a) and in the inset for type C16(2a) with $H/q|J| = 0.2$ and $J_3/q|J| = 1.0$ and -1.0, respectively.

The next two phase diagrams are for A10(2c) and A22(2c) types and are obtained for $H/q|J| = 1.75$ and $D/q|J| = -1.0, -1.9$ and presented in Figs.8(a) and 8(b), respectively. As seen from Fig.8(a), the first T_N lines start from higher negative values of $J_3/|J|$ and from higher temperatures and terminate at tricritical points where the T_t lines emerge which finally terminate at zero temperature about the same $J_3/|J|$ value for all q. During the existence of phase X no critical lines appear (since it is the FM phase and $H/q|J| \neq 0.0$), then we see the second T_N lines in semi-ellipsoidal shape which encloses the phase IV and are seen at higher $J_3/|J|$ for higher q. Finally we see the other FM phase I with no phase transition. Figure 8(b) is similar to Fig.8(a),

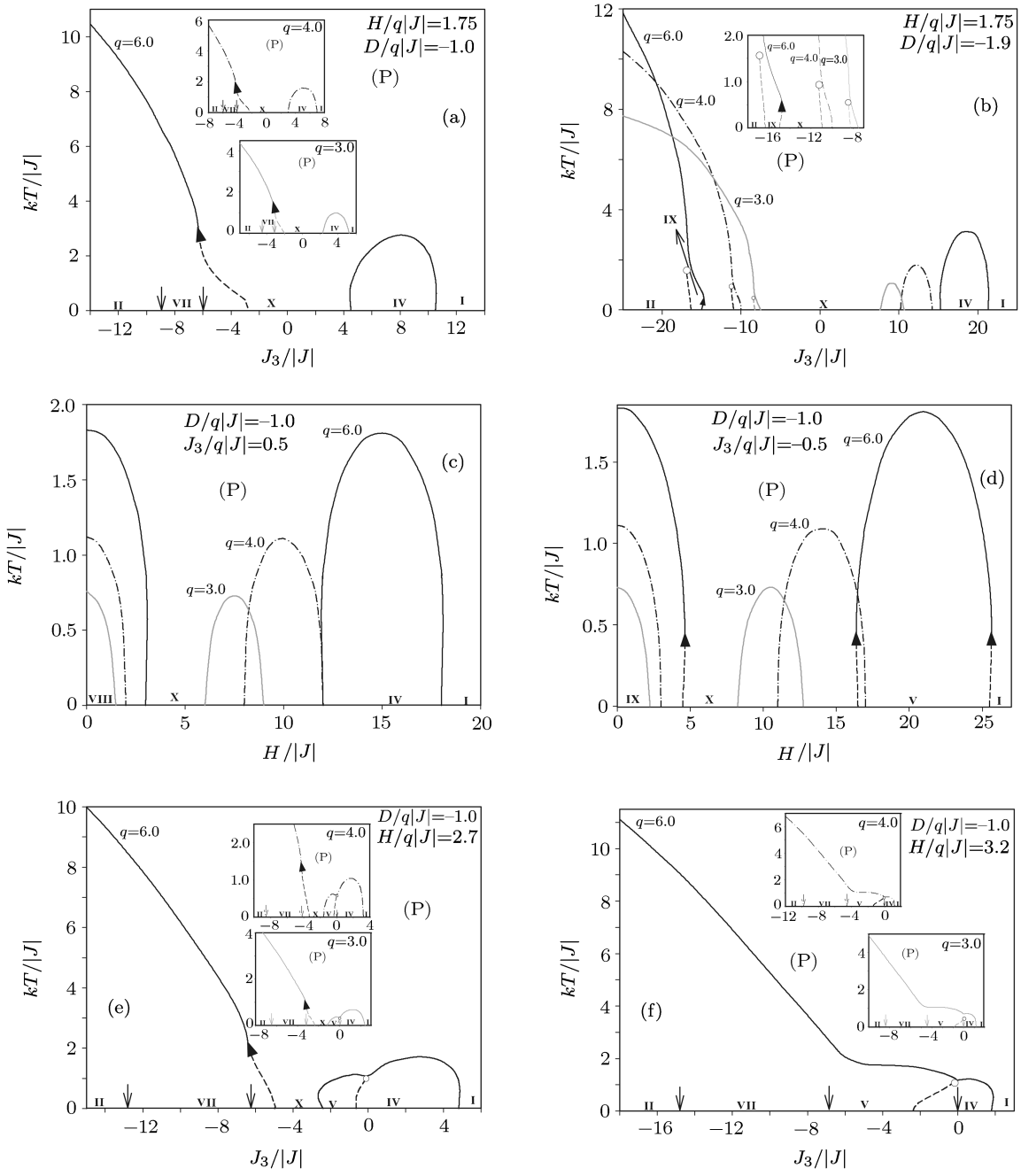


Fig.8. Phase diagrams of the model; (a) Type A10(2c) for $H/q|J| = 1.75$ and $D/q|J| = -1.0$ for q=6.0 and in the insets for q=3.0 and 4.0, (b) type A22(2c) for $H/q|J| = 1.75$ and $D/q|J| = -1.9$, (c) type B12(1c) for $D/q|J| = -1.0$ and $J_3/q|J| = 0.5$, (d) type B13(1c) for $D/q|J| = -1.0$ and $J_3/q|J| = -0.5$, (e) type A11(1c) for $D/q|J| = -1.0$ and $H/q|J| = 2.7$ for q=6.0 and insets for q=3.0 and 4.0 and (f) type A3(1c) for $D/q|J| = -1.0$ and $H/q|J| = 3.2$ for q=6.0 and insets for q=3.0 and 4.0.

but now the tricritical point is only seen for $q = 6$ and we also see the new type T_t lines terminating at isolated points on the left side of the first T_t lines for all q. In addition to these, the reentrant behaviour is only seen for $q = 6$ on both sides of the semi-ellipsoidal shape of both figures. It is clear that as $D/q|J|$ becomes more negative, the phase region X increases and thus the critical lines shift away from each other. The next two figures are for B12(1c) and B13(1c) types and obtained for $D/q|J| = -1.0$ and $J_3/q|J| = 0.5, -0.5$ and are illustrated in Figs.8(c) and 8(d), respectively. These two figures are actually similar to the previous two figures, but the first one only presents T_N lines and reentrant behaviour and is only seen on both sides of the semi-ellipsoids for $q = 6$, and the latter always presents tricritical points on the legs of only the first semi-ellipsoidal T_N lines for $q = 6$. Figure 8(e) is for A11(1c) type ($D/q|J| = -1.0$ and $H/q|J|$=2.7) similar to Fig.8(a), but now the semi-ellipsoidal T_N lines are somewhat corrupted and enclose phases V and IV which are separated with T_t lines terminating at isolated points for all q. Figure 8(f), is for the A3(1c) type with $D/q|J| = -1.0$ and $H/q|J|$=3.2, figure 8(e) shows the T_t lines, tricritical points and phase X have disappeared, instead the T_N line on the left now combines with the semi-closed T_N line on the right for all q. The T_t lines ending at isolated points still separate phases V and IV.

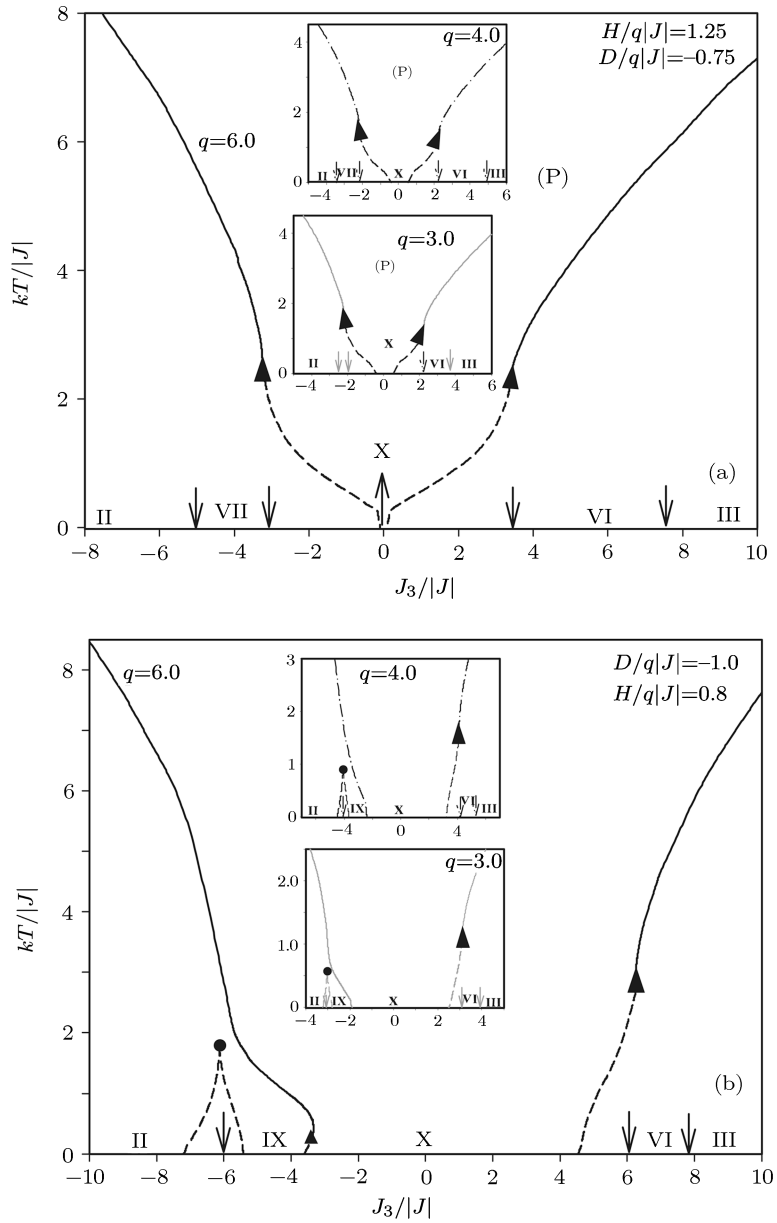


Fig.9. Phase diagrams; (a) Type A9(2b) with $H/q|J| = 1.25$ and $D/q|J| = -0.75$ for $q = 6.0$ and in the insets for q=3.0 and 4.0 and (b) Type A8(1c) with $D/q|J| = -1.0$ and $H/q|J| = 0.8$ for $q = 6.0$ and in the insets for q=3.0 and 4.0.

Figure 9(a) is obtained for $D/q|J| = -0.75$ and $H/q|J|$=1.25, and it is for A9(2b) type. The first T_N lines start from higher negative values of $J_3/|J|$ and from higher temperatures and terminate at tricritical points where the T_t lines emerge and finally terminate at zero temperature about the same $J_3/|J|$ value for all q. The second one almost symmetrical to the first one is also seen for positive values of $J_3/|J|$, thus we have now two tricritical points for each of q. Figure 9(b) is for A8(1c) type and obtained for $D/q|J| = -1.0$ and $H/q|J| = 0.8$, and it is also similar to Fig.9(a), but now the tricritical points are only seen for $q = 6$, i.e. almost symmetrical combinations of critical lines are only the T_N lines for $q = 3$ and 4. Two T_t lines combined at the double-critical end points are seen for all q in the negative region of $J_3/|J|$ only and inside which the phases II and IX coexist.

The final phase diagrams of this work exhibit one double-critical end point, two isolated points and four portions of the T_t lines in addition to one continuous T_N line for all q, and they are presented in Fig.10 (A7(2a) type and obtained for $D/q|J| = -1.0$ and $H/q|J| = 0.2$). The wing-shape T_N lines are almost symmetrical and centred at $J_3/|J| = 0.0$ for each q and seen at higher temperatures for higher q. Again the two T_t lines combined at the double-critical end points are seen for all q in the negative region of $J_3/|J|$ only, inside which phases II and IX coexist. On the right-hand side is contained only one T_t line which terminates at isolated points for all q, and the other T_t line is seen to be close to the centre of the T_N lines whose temperatures decrease and ends at zero temperature in the negative region of $J_3/|J|$ for all q again.

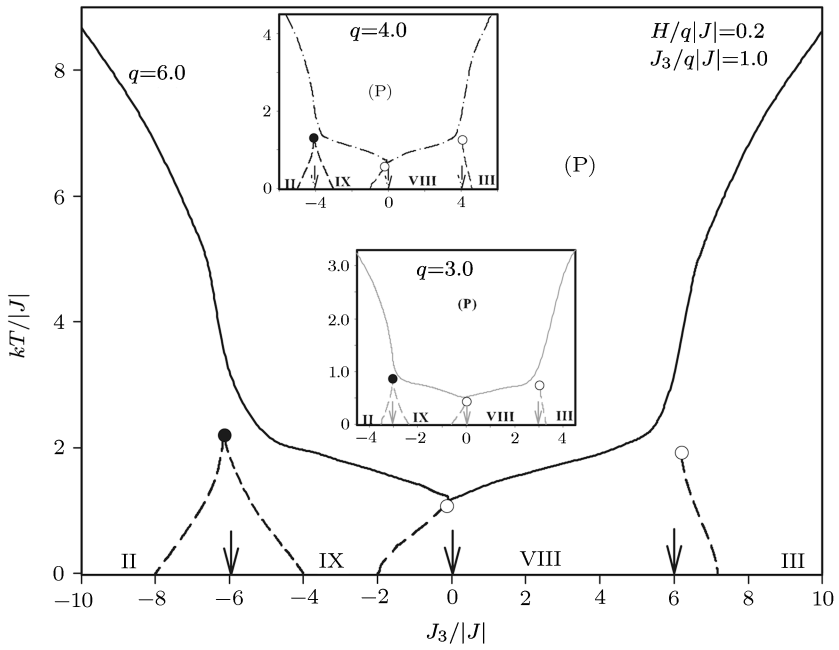


Fig.10. Phase diagram of type A7(2a) with $H/q|J| = 0.2$ and $D/q|J| = -1.0$ for q=6.0 and insets for q=3.0 and 4.0 separately.

In summary, the spin-3/2 Ising model is examined for the case of antiferromagnetic (AFM/AFM) interactions on the two-layer Bethe lattice by using the exact recursion relations in a pairwise approach for given coordination numbers q=3, 4 and 6 when the layers are under the influence of equal external magnetic and equal crystal fields. The ground state (GS) phase diagrams are obtained on the different planes in detail and then the temperature-dependent phase diagrams of the system are calculated accordingly. It is observed that the system presents both second- and first-order phase transitions for all q, therefore, tricritical points. It is also found that the system exhibits double-critical end points and isolated points. The model also presents two Néel temperatures, T_N, of which the existence leads to the reentrant behaviour.

Now we give a brief discussion of what we have found. (i) The existence of crystal fields has increased the number of the GS configurations compared with the case with no crystal field. (ii) The phases VIII, IX

and X are not seen in the GS phase diagram Fig.1(b), but these phases exist in Fig.1(c) where the crystal field is more negative. As a result, we can say that the strong crystal field drives the system towards spin-1/2 phase. (iii) The reentrant behaviour is seen for q=3.0, 4.0 and 6.0 when $D/q|J| = 0.0$, but when $D/q|J| \neq 0.0$ the reentrant behaviour is found only for $q = 4.0$ and 6.0. (iv) The double-critical end points and isolated points are not found for $D/q|J| = 0.0$, but with the addition of the crystal field they are also exhibited by our two-layer model. (v) The system exhibits double-critical end points for the phase transitions from phase II to phase IX as shown in Figs.9(b) and 10 for lower positive values of $H/q|J|$ and lower negative values of $D/q|J|$. But for higher positive values of $H/q|J|$ and higher negative values of $D/q|J|$, the double-critical end point is replaced with isolated point in Fig.8(b). (vi) The tricritical points are always seen for the phase transitions from any phase to phases I and X and the double-critical end points are only seen for the phase transitions from phase II to phase IX. Our final and well-known conclusion (vii) is that the temperatures of the phase transitions with the same system parameters increase with the increase of the coordination number, in addition to the increase in complexity and in diversity of the critical behaviours.

We should mention that was a very complicated and difficult task to complete, but our findings are very interesting and our efforts to study all the details are worth making. We should note that this is the first such work so we are unable to give any comparison, but we can at least give some comparisons for the case with spin-1 model: the GS configurations increase with the increase in spin values, i.e. 6 for spin-1 and 10 for spin-3/2, so the latter is more complicated as expected. The double-critical end points and isolated points are only seen for spin-3/2. In addition, the other critical behaviours such as the second- and first-order phase transitions and tricritical points for all q and the existence of the reentrant behaviour for only $q = 4$ and 6 are the same in both cases. Lastly, if we compare our case with the spin-3/2 FM/FM model[13] we also find some differences. For example, there are no tricritical points in previous work when $D = 0$ but it is found when $D \neq 0$ as in this work. The reentrant behaviour is not observed for the FM/FM cases in contrary to the AFM/AFM case.

References

[1] Sivardière J and Blume M 1972 *Phys. Rev.* B **5** 1126
[2] Krinsky S and Mukamel D 1975 *Phys. Rev.* B **11** 399
[3] Ferrenberg A M and Landau D P 1991 *J. Appl. Phys.* **70** 6215
[4] Li Z B, Shuai Z, Wang Q, Luo H J and Schu lke L 2001 *J. Phys.* A **34** 6069
[5] Oitmaa J and Enting I G 1975 *J. Phys.* A **8** 1097
[6] Lipowski A and Suzuki M 1993 *Physica* A **198** 227
[7] Jiang W, Wei G Z and Du A 2002 *J. Magn. Magn. Mater.* **250** 49
[8] Tucker J W, Balcerzak T, Gzik M and Sukiennicki A 1998 *J. Magn. Magn. Mater.* **187** 381
[9] Bahmad L, Benyoussef A and Ez-Zahraouy H 2004 *Surface Science* **552** 1
[10] Horiguchi T, Lipowski A and Tsushima N 1996 *Physica* A **224** 626
[11] Pan K K 2005 *Phys. Rev.* B **71** 134524
[12] Horiguchi T and Tsushima N 1997 *Physica* A **238** 295
[13] Albayrak E, Yilmaz S and Akkaya S 2007 *J. Magn. Magn. Mater.* **310** 98
Albayrak E, Yilmaz S and Akkaya S 2007 *Physica* A **381** 189
[14] Jaščur M and Kaneyoshi T 1995 *Physica* A **220** 542
[15] Htoutou K, Ainane A and Saber M 2004 *J. Magn. Magn. Mater.* **269** 245
[16] Hu C K, Izmailian N Sh and Oganesyan K B 1999 *Phys. Rev.* E **59** 6489
[17] Lyra M L and da Silva C R 1993 *Phys. Rev.* B **47** (1993) 526
[18] Monroe J L 2005 *Phys. Rev.* E **71** 017105
[19] Albayrak E, Yigit A and Akkaya S 2008 *J. Magn. Magn. Mater.* **320** 2241
[20] Albayrak E and Akkaya S 2009 *Phys. Scr.* **79** 065005
[21] Albayrak E, Akkaya S and Cengiz T *JMMM* in press
[22] Kurota M, Kikuchi R and Watari T 1953 *J. Chem Phys.* **21** 434
Domb C 1960 *Adv. Phys.* **9** 208
[23] Hu C K and Izmailian N Sh 1998 *Phys. Rev.* E **58** 1644
Izmailian N Sh and Hu C K *Physica* A **254** 198
[24] Tucker J W 1999 *J. Magn. Magn. Mater.* **195** 733
Albayrak E and Keskin M 2003 *J. Magn. Magn. Mater.* **261** 196
Albayrak E and Yigit A 2005 *Physica* A **349** 471
Albayrak E and Yigit A 2005 *Phys. Status Solidi* B **242** 1510
[25] Albayrak E and Keskin M 2000 *J. Magn. Magn. Mater.* **218** 121